Journal of Power Sources 245 (2014) 579–582

Contents lists available at SciVerse ScienceDirect

Journal of Power Sources

journal homepage: www.elsevier.com/locate/jpowsour

Short communication

Synthesis of three-dimensionally ordered macro-/mesoporous Pt with high electrocatalytic activity by a dual-templating approach

Chengwei Zhang [a], Hui Yang [a], Tingting Sun [a], Nannan Shan [a], Jianfeng Chen [a], Lianbin Xu [a,*], Yushan Yan [b]

[a] State Key Laboratory of Organic–Inorganic Composites, Beijing University of Chemical Technology, Beijing 100029, China
[b] Department of Chemical and Biomolecular Engineering, University of Delaware, Newark, DE 19716, USA

HIGHLIGHTS

- 3DOM/m Pt monoliths are synthesized by a dual-templating approach.
- 3DOM/m structure allows for both efficient mass transport and high surface area.
- 3DOM/m Pt exhibits larger ECSA (38.3 $m^2 g^{-1}$) than Pt black.
- 3DOM/m Pt shows improved electrocatalytic performance for MOR over Pt black.

ARTICLE INFO

Article history:
Received 22 April 2013
Received in revised form
28 June 2013
Accepted 30 June 2013
Available online 10 July 2013

Keywords:
Macro-/mesoporous structure
Platinum
Electrocatalyst
Colloidal crystal templating
Lyotropic liquid crystal
Methanol oxidation reaction

ABSTRACT

Three dimensionally ordered macro-/mesoporous (3DOM/m) Pt catalysts are fabricated by chemical reduction employing a dual-templating synthesis approach combining both colloidal crystal (opal) templating (hard-templating) and lyotropic liquid crystal templating (soft-templating) techniques. The macropore walls of the prepared 3DOM/m Pt exhibit a uniform mesoporous structure composed of polycrystalline Pt nanoparticles. Both the size of the mesopores and Pt nanocrystallites are in the range of 3–5 nm. The 3DOM/m Pt catalyst shows a larger electrochemically active surface area (ECSA), and higher catalytic activity as well as better poisoning tolerance for methanol oxidation reaction (MOR) than the commercial Pt black catalyst.

1. Introduction

Mesoporous metals with a high specific surface area, tailored pore structure and large electrical conductivity have attracted considerable attention for their applications in a variety of areas including catalysis, fuel cells, sensing, electronics, and magnetics [1–5]. Template-directed methods based on hard templates (e.g. mesoporous silica) or soft templates (e.g. lyotropic liquid crystals (LLC) made of nonionic surfactants) are commonly used to fabricate mesoporous metals [5–9]. Among the mesoporous metals, mesoporous Pt is of great importance due to its high chemical stability and unique catalytic properties [10–12].

Hierarchically macro-/mesoporous materials have received growing interest since they combine the advantages of efficient mass transport for molecules from the macropores and high surface area from the mesopores [13,14]. Various synthesis strategies have been developed to fabricate hierarchically macro-/mesoporous materials. The dual-templating synthesis approach employing a combination of both surfactant and colloidal crystal (opal) templating techniques offers a promising way for the fabrication of materials with three-dimensionally (3D) ordered macropores and mesopores. However, there have been very few studies conducted on the production of 3D ordered macro-/mesoporous (3DOM/m) metallic materials [14]. 3DOM/m Pt thin films were first prepared by Yamauchi and Kuroda via electrodeposition in LLC of nonionic surfactant $C_{16}EO_8$ using polystyrene (PS) opal as a mold [15]. 3DOM/m Pt monoliths are also technologically important because of their ease of handling, larger scale synthesis,

* Corresponding author. Tel.: +86 10 64449241; fax: +86 10 64434784.
E-mail addresses: xulb@mail.buct.edu.cn, lbxu99@163.com (L. Xu).

0378-7753/$ – see front matter © 2013 Elsevier B.V. All rights reserved.
http://dx.doi.org/10.1016/j.jpowsour.2013.06.162

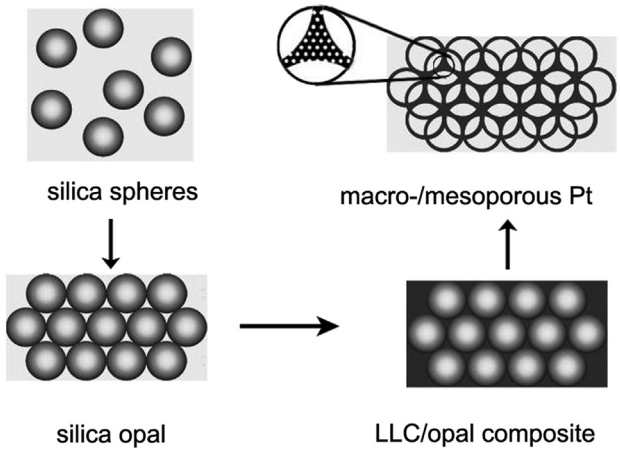

Scheme 1. Schematic of the fabrication of three dimensional ordered macro-/mesoporous (3DOM/m) Pt.

and potential applications in catalysis and battery electrodes. In this work, we report for the first time the synthesis of 3DOM/m Pt monoliths by chemical reduction using silica opal as a hard template and LLC of the nonionic surfactant Brij 56 ($C_{16}H_{34}(OCH_2CH_2)_{10}$) as a soft template for mesostructure, and investigate their electrocatalytic properties for methanol oxidation reaction (MOR).

2. Experimental

Scheme 1 illustrates the procedure for the fabrication of 3DOM/m Pt catalysts. Silica opal templates were prepared by previously published methods [16], through the gravity sedimentation of monodisperse silica colloids into close-packed structures. In this study, the highly ordered single-crystal-like opal pieces were composed of ca. 290 nm silica spheres. To prepare the 3DOM/m Pt catalyst, a piece of silica opal was first immersed in the precursor solution containing nonionic surfactant Brij 56, $H_2PtCl_6 \cdot H_2O$, H_2O, and C_2H_5OH (0.21:0.14:0.15:0.5 in mass ratio). Through the evaporation of ethanol at 25 °C, the lyotropic liquid crystal (LLC) was gradually formed, and the void space of opal was filled with LLC containing Pt ions. After that, the LLC filled opal was carefully removed from the bulk LLC phase, and then reduced by dimethylamine borane (DMAB) through the vapor infiltration of DMAB into the LLC/opal composite and keeping at 25 °C for 24 h in a closed vial [17]. The freestanding 3DOM/m Pt was obtained by removing the opal silica spheres with a 5 wt.% HF solution (24 h).

The prepared 3DOM/m Pt was characterized by scanning electron microscopy (SEM, Hitachi S-4700), transmission electron microscopy (Hitachi H800), high-resolution TEM (HR-TEM, JEOL JEM-3010), and selected area electron diffraction (SAED, JEOL JEM-3010).

All the electrochemical experiments (cyclic voltammetry (CV), linear sweep voltammetry (LSV), and chronoamperometry) were carried out in a potentiostat/galvanostat (Reference 600, Gamry Instruments) using a conventional three-electrode cell with a glassy carbon (GC) electrode (4 mm in diameter) as the work

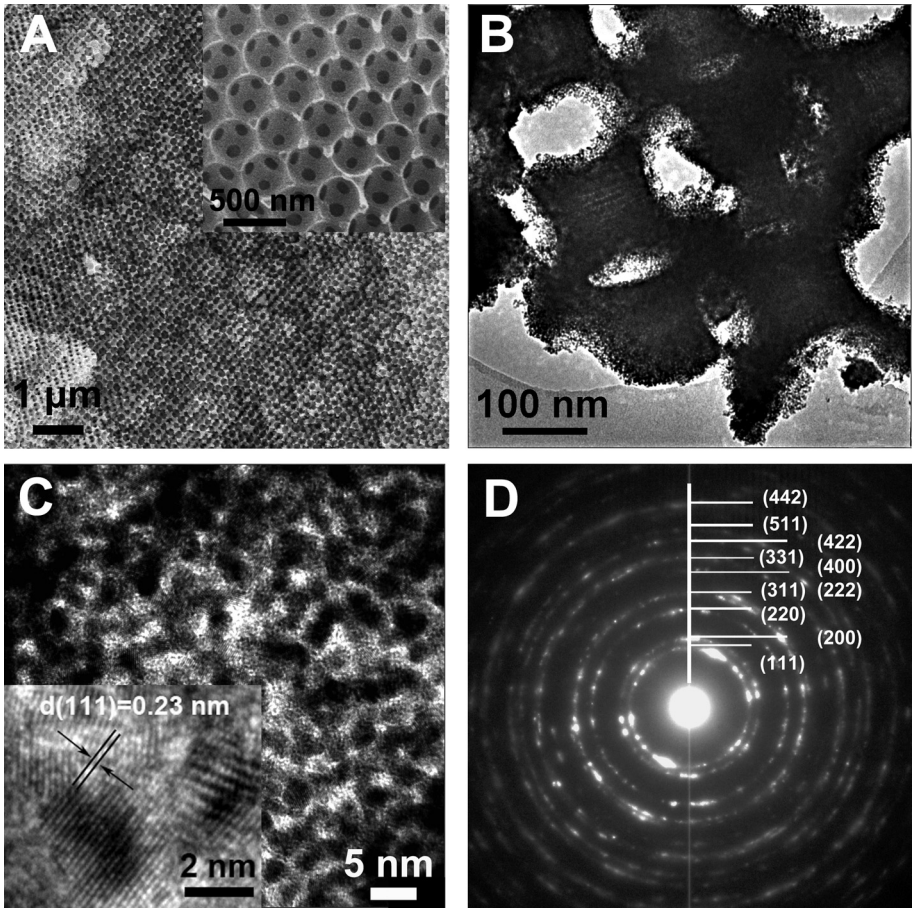

Fig. 1. (A) SEM image of the 3DOM/m Pt after the removal of the opal template; inset: higher magnification SEM image with (111) orientation. (B) TEM image of the 3DOM/m Pt. (C) HR-TEM image of the macropore wall; inset: higher magnification image showing the lattice fringes. (D) SAED pattern of the 3DOM/m Pt.

electrode, a double junction Ag/AgCl (saturated KCl) electrode as the reference electrode, and a Pt flag as the counter electrode. All electrode potentials were converted to the normal hydrogen electrode (NHE) scale using $E_{NHE} = E_{Ag/AgCl;\ sat.\ KCl} + 0.197$ V. The working electrode was prepared as follows. The GC electrode was polished to a mirror finish using aqueous alumina suspensions and cleaned by ultrasonication in deionized water. 5 mg of catalyst (i.e 3DOM/m Pt, or commercial Pt black (HiSpec1000, Johnson Matthey)) was ultrasonically dispersed in 0.5 mL ethanol. A volume of 10 μL of the mixture solution was then pipetted onto the GC substrate. After drying at 80 °C, 5 μL of Nafion solution (5 wt.%) was pipetted on the GC substrate and dried completely. The CV, LSV and chronoamperometry tests were performed in argon-purged 0.5 M H_2SO_4 solution with or without 1 M CH_3OH at room temperature.

3. Results and discussion

Fig. 1A shows the typical SEM image of the 3DOM/m Pt catalyst produced from the silica opal template. The 3DOM/m Pt exhibits a uniform macroporous structure that is the inverse of the original opal, and the size of the macropores is ca. 290 nm, which is consistent with the diameter of the original silica spheres, indicating that the 3DOM/m Pt does not contract after the removal of opal. The hierarchically macro-/mesoporous structure can be seen from the TEM image (Fig. 1B) of the 3DOM/m Pt. The HR-TEM image (Fig. 1C) reveals that the coexistence of porous mesostructure and Pt nanocrystallites in the macropore walls. Both the size of the mesopores and Pt nanocrystallites are in the range of 3–5 nm. The lattice fringes with 0.23 nm spacing (inset of Fig. 1C) are observed in the mesopore walls, corresponding to the d-spacing between adjacent (111) crystallographic planes of Pt. The SAED pattern exhibits polycrystalline face-centered cubic (fcc) Pt feature with homogenous diffraction rings (Fig. 1D), which corresponds to the presence of many small Pt particles in the macropore walls (Fig. 1C).

Fig. 2A shows the cyclic voltammograms (CVs) in 0.5 M H_2SO_4 solution. The voltammetric features are in good agreement with the literature [11,15,18]. The electrochemically active surface area (ECSA) of Pt was estimated by the area of desorption of atomic hydrogen on the curve of the CV between 0 and 0.35 V. The ECSA of the catalyst can be calculated by the relation $ECSA = Q_H/(m \cdot c)$ [19,20] where Q_H is the charge for hydrogen desorption (mC cm^{-2}), m is the Pt loading (mg cm^{-2}) in the electrode, and c is the charge required for the monolayer adsorption of hydrogen on a Pt surface (0.21 mC cm^{-2}). The ECSA of mesoporous Pt is calculated to be 38.3 $m^2\ g^{-1}$, which is higher than that of the commercial Johnson Matthey Pt black (21.5 $m^2\ g^{-1}$), and comparable to that of the mesoporous Pt particles reported in the literature [21].

To characterize the electrochemical performance, the 3DOM/m Pt catalyst was explored as an electrocatalyst for methanol oxidation reaction (MOR). The CVs obtained in 0.5 M H_2SO_4 and 1 M CH_3OH solution at a scan rate of 50 mV s^{-1} are shown in Fig. 2B. The current density of the methanol oxidation for the 3DOM/m Pt reaches a peak value of 0.31 A mg^{-1} in the forward scan, which is much higher than that of the Pt black (0.10 A mg^{-1}). The higher methanol oxidation mass activity of the 3DOM/m Pt catalyst could be attributed to the greatly increased ECSA [22]. After normalization to the ECSA (Fig. 2C), the peak current density of the 3DOM/m^{-1} Pt (0.81 mA cm^{-2}) is also higher than that of the Pt black (0.46 mA cm^{-2}). These results demonstrate that the 3DOM/m Pt exhibits much higher catalytic activity than the Pt black in terms of both mass and area specific activities, which may be attributed to the more exposed active sites owing to the hierarchically macro-/mesoporous structure, and good permeability due to the 3D interconnected macropores [12,23,24].

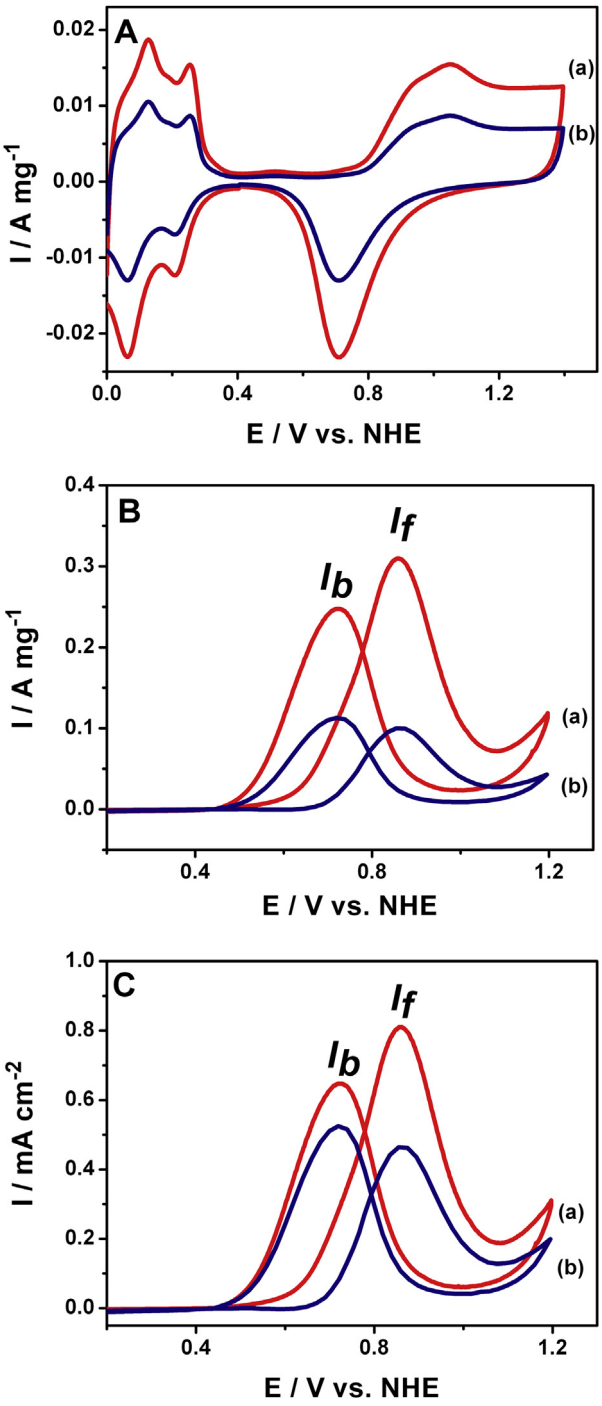

Fig. 2. (A) Cyclic voltammograms (CVs) of the 3DOM/m Pt catalyst (a) and Pt black (b) in 0.5 M H_2SO_4. (B) CVs of the 3DOM/m Pt catalyst (a) and Pt black (b) in 0.5 M H_2SO_4 and 1 M CH_3OH. (C) ECSA-normalized CVs of the 3DOM/m Pt catalyst (a) and Pt black (b) in 0.5 M H_2SO_4 and 1 M CH_3OH. All the scan rates are 50 mV s^{-1}.

In addition, the ratio of I_f (the peak current of the forward scan) to I_b (the peak current of the backward scan) of the catalyst is another important performance parameter. The I_f/I_b is generally used to evaluate the catalyst tolerance to carbonaceous species accumulation. From Fig. 2B, the I_f/I_b of mesoporous Pt is 1.25, which is higher than that of the Pt black catalyst (0.90). A higher I_f/I_b indicates better oxidation of methanol to carbon dioxide during the anodic scan and less accumulation of carbonaceous residues on the catalyst surface. This higher I_f/I_b reveals that the 3DOM/m Pt

catalyst has better tolerance for poisoning of carbonaceous species than Pt black [7]. This may be attributed to the highly porous structure of the 3DOM/m Pt which can improve the mass transfer effect and offer more activity sites that are helpful for activating H_2O molecule to act as an oxygen source which could promote the oxidation of the intermediate poisoning species [25,26].

To further investigate the electrocatalytic properties of the catalysts, the linear sweep voltammograms (LSVs) and chronoamperomograms were measured in 0.5 M H_2SO_4 and 1 M CH_3OH solution. In the LSVs (Fig. 3A), the onset potential for the 3DOM/m Pt occurred at about 0.27 V, which was relatively more negative than that of the Pt black (about 0.44 V), indicating higher catalytic activity of the 3DOM/m Pt for the MOR. Moreover, at any given oxidation current density (e.g., as indicated by dashed line in Fig. 3A), the corresponding oxidation potential on the 3DOM/m Pt catalyst was obviously lower than that on the Pt black, further suggesting that the MOR was easier to perform on the 3DOM/m Pt catalyst surface. The exact causes for the improved MOR activity are not clear at this time, but the possible factors are that, compared with the Pt black, the 3DOM/m Pt has compression strain which can lower the CO binding energy [27] and thus facilitate the MOR, and more edge sites that are also helpful for water dissociation [26]. Both CO oxidation and water dissociation are important and necessary steps for efficient MOR [28]. The chronoamperomograms (Fig. 3B) recorded at 0.8 V for 2000 s indicated that the current density of the 3DOM/m Pt was higher than that of the Pt black over the entire time range, also revealing the improved electrocatalytic performance of the 3DOM/m Pt catalyst in the MOR.

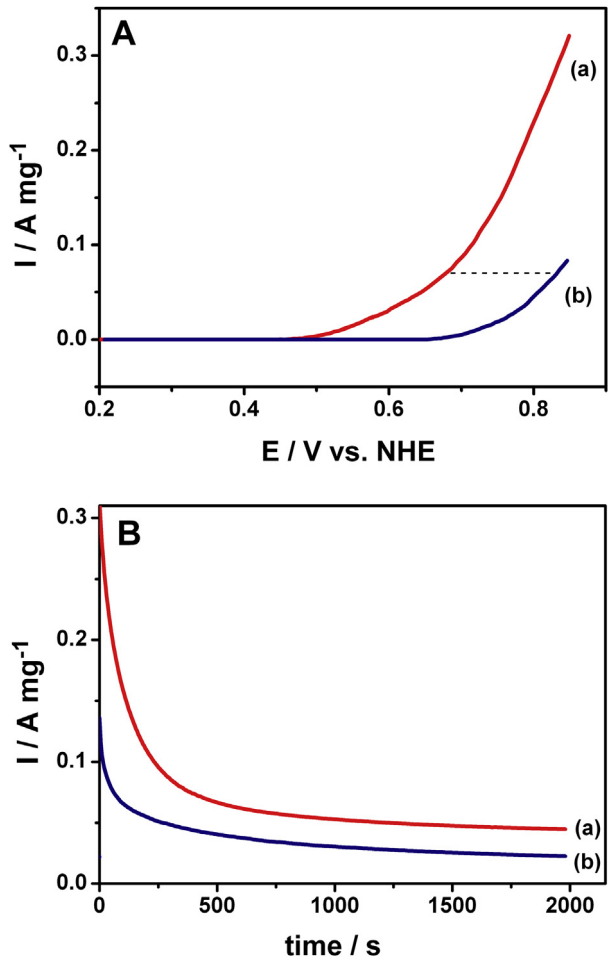

Fig. 3. (A) Linear sweep voltammograms (LSVs) and (B) chronoamperomograms for methanol oxidation reaction catalyzed by 3DOM/m Pt (a) and Pt black (b) in 0.5 M H_2SO_4 and 1 M CH_3OH. The scan rate of the LSVs is 5 mV s^{-1}, and the chronoamperomograms were recorded at 0.8 V.

4. Conclusions

In summary, 3DOM/m Pt catalysts have been successfully synthesized by a dual-templating technique using silica opal as a macropore template and the nonionic surfactant Brij 56 LLC as a mesopore template. The macropore walls of the prepared 3DOM/m Pt exhibit a uniform mesoporous structure composed of polycrystalline Pt nanoparticles. The 3DOM/m Pt catalyst shows a larger electrochemically active surface area, and higher electrocatalytic activity as well as better poisoning tolerance for methanol oxidation reaction (MOR) than that of the commercial Pt black catalyst. It is expected that the present method can be extended to prepare other 3DOM/m metals (e.g. Ni, Pd, and Ru) or alloys (e.g. Pt–Ni, and Pt–Ru alloys).

Acknowledgments

The authors gratefully acknowledge financial support from the National 973 Program of China (2009CB219903), and the National Natural Science Foundation of China (51172014 and 20971012).

Appendix A. Supplementary data

Supplementary data related to this article can be found at http://dx.doi.org/10.1016/j.jpowsour.2013.06.162.

References

[1] Y. Yamauchi, N. Suzuki, L. Radhakrishnan, L. Wang, Chem. Rec. 9 (2010) 321–339.
[2] S.C. Warren, L.C. Messina, L.S. Slaughter, M. Kamperman, Q. Zhou, S.M. Gruner, F.J. DiSalvo, U. Wiesner, Science 320 (2008) 1748–1752.
[3] E.A. Franceschini, G.A. Planes, F.J. Williams, G.J.A.A. Soler-Illia, H.R. Corti, J. Power Sources 196 (2011) 1723–1729.
[4] S. Daniele, C. Bragato, D. Battistel, Electroanalysis 24 (2012) 759–766.
[5] H. Wang, L. Wang, T. Sato, Y. Sakamoto, S. Tominaka, K. Miyasaka, N. Miyamoto, Y. Nemoto, O. Terasaki, Y. Yamauchi, Chem. Mater. 24 (2012) 1591–1598.
[6] H. Wang, M. Imura, Y. Nemoto, S.-E. Park, Y. Yamauchi, Chem. Asian J. 7 (2012) 802–808.
[7] L. Wang, Y. Yamauchi, Chem. Eur. J. 17 (2011) 8810–8815.
[8] Y. Yamauchi, K. Kuroda, Chem. Asian J. 3 (2008) 664–676.
[9] K.-R. Lee, M.-H. Kim, J.-E. Hong, Y.-U. Kwon, J. Raman Spectrosc. 44 (2013) 6–11.
[10] J. Kibsgaard, Y. Gorlin, Z. Chen, T.F. Jaramillo, J. Am. Chem. Soc. 134 (2012) 7758–7765.
[11] C.L. Lee, C.C. Wu, H.P. Chiou, C.M. Syu, C.H. Huang, C.C. Yang, Int. J. Hydrogen Energy 36 (2011) 6433–6440.
[12] Y. Zhong, C.L. Xu, L.B. Kong, H.L. Li, Appl. Surf. Sci. 255 (2008) 3388–3393.
[13] X.-Y. Yang, Y. Li, A. Lemaire, J.-G. Yu, B.-L. Su, Pure Appl. Chem. 81 (2009) 2265–2307.
[14] B.-L. Su, C. Sanchezl, X.-Y. Yang, Hierarchically Structured Porous Materials, Wiley-VCH, Weinheim, 2012.
[15] Y. Yamauchi, K. Kuroda, Electrochem. Commun. 8 (2006) 1677–1682.
[16] J. Chen, Z. Hua, Y. Yan, A.A. Zakhidov, R.H. Baughman, L. Xu, Chem. Commun. 46 (2010) 1872–1874.
[17] Y. Yamauchi, A. Takai, T. Nagaura, S. Inoue, K. Kuroda, J. Am. Chem. Soc. 130 (2008) 5426–5427.
[18] A. Takai, Y. Yamauchi, K. Kuroda, J. Am. Chem. Soc. 132 (2010) 208–214.
[19] A. Pozio, M. De Francesco, A. Cemmi, F. Cardellini, L. Giorgi, J. Power Sources 105 (2002) 13–19.
[20] S.H. Sun, G.X. Zhang, D.S. Geng, Y.G. Chen, R.Y. Li, M. Cai, X.L. Sun, Angew. Chem. Int. Ed. 50 (2011) 422–426.
[21] J.H. Jiang, A. Kucernak, J. Electroanal. Chem. 533 (2002) 153–165.
[22] G.H. Yang, Y.J. Li, R.K. Rana, J.J. Zhu, J. Mater. Chem. A 1 (2013) 1754–1762.
[23] L. Wang, Y. Yamauchi, Chem. Mater. 21 (2009) 3562–3569.
[24] S.Z. Wang, L. Kuai, Y.C. Huang, X. Yu, Y.D. Liu, W.Z. Li, L. Chen, B.Y. Geng, Chem. Eur. J. 19 (2013) 240–248.
[25] A. Kucernak, J.H. Jiang, Chem. Eng. J. 93 (2003) 81–90.
[26] X.Y. Zhang, W. Lu, J.Y. Da, H.T. Wang, D.Y. Zhao, P.A. Webley, Chem. Commun. (2009) 195–197.
[27] M. Mavrikakis, B. Hammer, J.K. Nørskov, Phys. Rev. Lett. 81 (1998) 2819–2822.
[28] S.W. Lee, S. Chen, W. Sheng, N. Yabuuchi, Y.-T. Kim, T. Mitani, E. Vescovo, Y. Shao-Horn, J. Am. Chem. Soc. 131 (2009) 15669–15677.